

Effect of Er, Gd, and Nd Co-Dopants on the Properties of Sm-Doped Ceria Electrolyte for IT-SOFC



ALIYE ARABACI

Doped ceria electrolytes of $\text{Ce}_{0.8}\text{Sm}_{0.20}\text{O}_{1.90}$ (SDC), $\text{Ce}_{0.8}\text{Er}_{0.08}\text{Sm}_{0.12}\text{O}_{1.90}$ (ESDC), $\text{Ce}_{0.8}\text{Gd}_{0.08}\text{Sm}_{0.12}\text{O}_{1.90}$ (GSDC), and $\text{Ce}_{0.8}\text{Nd}_{0.08}\text{Sm}_{0.12}\text{O}_{1.90}$ (NSDC) were prepared by a citric–nitrate combustion process. The thermal decomposition of the precursor was investigated by simultaneous thermogravimetric analysis and differential thermal analysis experiments. The phase structure of the calcined and sintered powders was characterized by X-ray diffraction analysis. All of the samples were fluorite-type ceria-based solid solutions. The calcined and sintered powders were also characterized by Fourier transform infrared spectroscopy. Scanning electron microscopy was used to characterize the samples after calcination and sintering. A relative density over 95 percent of the theoretical density was achieved after the sintering process. Electrical conductivities of the sintered samples were measured using the impedance spectra method. The highest ionic conductivity value was found to be $5.28 \times 10^{-2} \text{ S cm}^{-1}$ at 1023 K (750 °C) for GSDC sintered at 1673 K (1400 °C) for 6 hours.

DOI: 10.1007/s11661-017-3990-4

© The Minerals, Metals & Materials Society and ASM International 2017

I. INTRODUCTION

THE solid oxide fuel cell (SOFC) is one of the most attractive energy conversion devices because of its high efficiency, flexibility of fuel choice, and environmental friendliness. In general, conventional SOFC systems, which use yttria-stabilized zirconia (YSZ) as an electrolyte for their high conversion efficiency, are operated at approximately 1273 K (1000 °C). However, at such high operating temperatures, there are some problems, such as interfacial reaction between the components, mechanical and thermal degradation, thermal expansion mismatch, and high cost of materials.^[1–4] Therefore, it is necessary to lower [773 K to 1073 K (500 °C to 800 °C)] the operating temperature of the SOFCs. Ceria doped with a tri-valent cation, such as, Sm^{3+} , Gd^{3+} , and Nd^{3+} , is a potential electrolyte for solid oxide fuel cell applications at temperatures below 1073 K (800 °C) because of its appreciable oxygen ion conductivity above 873 K (600 °C).^[1,5–7]

In particular, ceria doped with samarium oxide and gadolinium oxide was found to have the highest electrical conductivity at a fixed dopant level because the corresponding distortions of the ceria lattice are the smallest.^[8] Kim^[9] found that the expansion of the lattice deviation of the doped ceria from pure ceria would lead to an increase of the lattice strain of doped ceria, thereby resulting in an increase of the activation energy of

conduction and a decrease of the ionic conductivity of the doped ceria.

To further improve the ionic conductivity of ceria, some co-doped ceria-based electrolytes have been studied.^[10–16] Yamamura and coworkers^[10] found that co-doping might suppress the ordering of oxygen vacancies and therefore lower the activation energy of conduction and improve the ionic conductivity. Moreover, Wang and coworkers suggested that ceria co-doped with two elements has a higher electrical conductivity in comparison with single element-doped ceria.^[12] Andersson *et al.*^[13] reported that, among all rare earth-doped ceria materials, Nd^{3+} and Sm^{3+} co-doped ceria or Pr^{3+} and Gd^{3+} co-doped ceria should have the highest electrical conductivity. They applied quantum-mechanical first-principles methods to simulate the crystal structure and calculate the activation energy of oxygen vacancies within all types of rare earth-doped ceria materials. They reached a conclusion that the optimized dopants in ceria should have an effective atomic number between 61 (Pm) and 62 (Sm). Mori *et al.*^[14] found that the ionic conductivity of $(\text{La}_{0.75}\text{Sr}_{0.2}\text{Ba}_{0.05})_{0.175}\text{Ce}_{0.825}\text{O}_{1.891}$ was higher than that of the single element-doped ceria. Similarly, Van Herle *et al.*^[15] stated that co-doped ceria with three, five, or ten dopants showed a considerably higher conductivity in air than the best single element-doped material with the same oxygen vacancy concentration. Wang *et al.* suggested that $\text{Ce}_{0.85}\text{Gd}_{0.1}\text{Mg}_{0.05}\text{O}_{1.9}$ electrolyte provides evidence for the co-doping method that could enhance the ionic conductivity.^[16] However, Yoshida *et al.*^[17,18] found that ceria co-doped with La^{3+} and Y^{3+} did not show any synergistic effects on ionic conductivity. Thus, inconsistent results are found in the literature on the co-doping effect. Therefore, there is a need for further

ALIYE ARABACI is with the Department of Metallurgical Engineering, Faculty of Engineering, Istanbul University, Avcilar 34320, Istanbul, Turkey. Contact e-mail: aliye@istanbul.edu.tr

Manuscript submitted December 15, 2015.

Article published online February 10, 2017

research to optimize the type of the dopant element and to understand how they affect the ionic properties of ceria.

Composition and microstructure play important roles on improving ionic conductivity.^[19,20] The ionic conductivity of doped ceria increases with increasing dopant concentration before reaching a maximum level and then decreasing at higher dopant concentrations because of the formation of micro-domains. At higher dopant amounts, oxygen vacancies become associated with the dopant cations and the oxygen-ion mobility decreases. It has been stated that the ionic conductivity reaches a maximum at a dopant cation concentration of approximately 20 mol pct, depending on the dopant element.^[1,21,22]

From the previous studies,^[23–25] it was understood that 10 mol pct to 20 mol pct is the critical dopant range. Micro-domain formation is observed beyond this level because of the high-temperature exposure. The doping cations Sm^{3+} , Y^{3+} , and Nd^{3+} have a tendency to form large clusters with oxygen vacancies. For the doping cation Er^{3+} , the critical dopant concentration was reported to be approximately 10 mol pct to achieve the best total conductivity value for ceria. When Er^{3+} was doped higher than 10 mol pct, an additional phase, Er_2O_3 , forms, and this situation causes a decrease in the conductivity of ceria.^[7] There is a limited scope of research that has been conducted to date regarding Er co-doped ceria. In our previous work,^[26] the $\text{Ce}_{0.82}\text{Gd}_{0.1}\text{Er}_{0.08}\text{O}_{1.91}$ composition showed the highest ionic conductivity. Therefore, in the present study, the mol pct of Nd^{3+} , Gd^{3+} , and Er^{3+} dopant cations was selected as 8 pct for the prepared concentrations. The total dopant cation amount was kept at 20 mol pct, having the general Formula $\text{Ce}_{0.8}\text{RE}_{0.08}\text{Sm}_{0.12}\text{O}_{1.90}$ (RE^{3+} : Gd^{3+} , Nd^{3+} , Er^{3+}).

In addition, both phase purity and relative density are important factors for obtaining high performance doped cerium oxide electrolytes. Doped ceria powder can be synthesized using various techniques, such as hydrothermal methods and combustion.^[27–31] These wet chemical processes are able to produce ultrafine powders with narrow size distributions. Among the available wet chemical processes, combustion synthesis is capable of obtaining an ultrafine powder of doped cerium oxide efficiently and economically.^[29–31] Citric acid is one of the most inexpensive organic acids and is used as fuel in the combustion reaction. Citric acid is known to act as a complexing agent for a number of metal ions as it has three carboxyl groups and one hydroxyl group.

In this study, $\text{Ce}_{0.8}\text{Er}_{0.08}\text{Sm}_{0.12}\text{O}_{1.90}$ (ESDC), $\text{Ce}_{0.8}\text{Gd}_{0.08}\text{Sm}_{0.12}\text{O}_{1.90}$ (GSDC), $\text{Ce}_{0.8}\text{Nd}_{0.08}\text{Sm}_{0.12}\text{O}_{1.90}$ (NSDC), and $\text{Ce}_{0.8}\text{Sm}_{0.20}\text{O}_{1.90}$ (SDC) materials were prepared by using a citric–nitrate combustion process (CNC), and then the resulting materials were characterized. The effect of the co-doping element on the structural properties and on the ionic conductivity was compared to single element-doped ceria ($\text{Ce}_{0.8}\text{Sm}_{0.20}\text{O}_{1.90}$). The purpose was to develop new ceria-based solid electrolyte materials with further improved ionic conductivities.

II. EXPERIMENTAL

Cerium nitrate [$\text{Ce}(\text{NO}_3)_3 \times 6\text{H}_2\text{O}$, purity 99.99 pct, Sigma aldrich], samarium nitrate [$\text{Sm}(\text{NO}_3)_3 \times 6\text{H}_2\text{O}$, purity 99.99 pct, Sigma Aldrich], erbium nitrate [$\text{Er}(\text{NO}_3)_3 \times 5\text{H}_2\text{O}$, purity 99.9 pct, Sigma Aldrich], and neodymium nitrate [$\text{Nd}(\text{NO}_3)_3 \times 6\text{H}_2\text{O}$, purity 99.9 pct, Sigma aldrich] were used as the starting materials. To prepare the SDC, ESDC, GSDC, and NSDC electrolyte samples, the nitrate salts were weighed and then dissolved in deionized water to the desired concentrations. Citric acid anhydrous ($\text{C}_6\text{H}_8\text{O}_7$, Boehringer Ingelheim) was added to the mixed nitrate solutions as a fuel. The molar ratio of metal nitrates to citric acid was set to 1:1. The solutions were heated and stirred on a hot plate at 358 K (85 °C) for approximately 2 hours to form a viscous gel. After heating for a longer time at 358 K (85 °C), the gel swelled into a voluminous light brown foam and then auto-ignition of the light brown foam occurred, accompanied with the evolution of a large number of gaseous molecules. Afterwards, this foam was kept at 573 K (300 °C) for 1 hours in a muffle furnace, and then the powders obtained were calcined at 873 K (600 °C) for 3 hours in the muffle furnace to remove the carbon residues and form a well crystalline structure.

The thermal decomposition of the dried gel precursor (a piece of viscous gel was dried in an oven at 343 K (70 °C) for 24 hours) was investigated using differential thermal analysis (DTA) and thermogravimetric analysis (TGA), which were performed in the temperature range 300 K to 1073 K (27 °C to 800 °C) with an SII Exstar 6000 TG/DTA 6300 device at a heating rate of 5 K/min (5 °C/min) in an air atmosphere.

The calcined powders were characterized by X-ray diffraction (Rigaku D/Max-2200 PC) for phase analysis. The average crystallite diameter of the calcined samples was calculated by using the Scherrer method, $d = K\lambda/\beta\cos\theta$, where K is a constant taken to be 0.9, d is the crystallite size (nm), λ is the wavelength of the radiation (1.5418 Å), β is the corrected peak at the full width at half maximum (FWHM) intensity and θ is the scattering angle of the main reflection, (111).

Next, the calcined powders were isostatically cold-pressed under 200 MPa to prepare green pellets. The pellets were heated at 1673 K (1400 °C) for 4 hours in air and then furnace cooled. Microstructural analysis of the sintered samples was conducted using an FEI-QUANTA FEG 450 scanning electron microscope (SEM).

To identify the crystal structure of the sintered samples, XRD analysis was performed. The Archimedes method was used to measure the relative density of the sintered samples. The structural features of the calcined and sintered SDC, ESDC, GSDC, and NSDC powders were characterized by Perkin-Elmer FTIR (Spectrum 100) spectroscopy using the KBr pellet method over the range 400 to 4000 cm^{-1} .

Impedance was measured using the two-probe method with an AC impedance analyzer (Solartron 1260 FRA and 1296 Interface) as a function of temperature [573 K to 1073 K (300 °C to 800 °C)] in air in the measuring frequency range from 100mHz to

10MHz. The impedance data were analyzed using the Zview software. Silver paste is one of the most commonly used conductive pastes to obtain a conductive surface. There is no side-effect of silver electrode use for high temperatures, *e.g.*, 1073 K (800 °C).^[11,26,32] Therefore, silver conductive paste (Sigma Aldrich) was applied on to each side of the sintered pellets for the purpose of signal collection. Next, these pellets were heated to 1073 K (800 °C) and kept at this temperature for 30 min to produce solid silver electrodes on both sides of the pellets. Curve fitting and resistance calculation were performed using Zview software. The resistance data for each sample measured at different temperatures are converted to conductivity data using the relation shown in the following equation:

$$\sigma = \frac{l}{A \cdot R_{\text{Total}}} \quad [1]$$

where l is the thickness, R_{Total} ($R_{\text{Total}} = R_{\text{Gi}}$ (the grain interior (lattice) resistance) + R_{Gb} (the grain boundary resistance)) is the total resistance and A is the effective electrode area.

The temperature dependence of conductivity can be expressed by the following equation:

$$\sigma = \frac{\sigma_0}{T} e^{-\frac{(E_a + \Delta H_m + \Delta H_a)}{kT}} \quad [2]$$

where T is the temperature in K; σ is the total conductivity at temperature T ; σ_0 is a pre-exponential factor; E_a is the activation energy, and k is Boltzmann's constant. ΔH_m and ΔH_a denote the migration enthalpy and association enthalpy of the oxygen vacancy, respectively. σ_0 is related to the oxygen vacancy concentration and vibrational frequency of the lattice.

III. RESULT AND DISCUSSION

A. TG-DTA Analysis

Figure 1 shows the simultaneous TGA and DTA plots obtained from a piece of viscous gel, which was dried in an oven before the analyses. Gel combustion is an exothermic reaction between an oxidizer and a fuel. Metal nitrates act as the oxidizer, and citric acid is the fuel in this study. The TGA/DTA curve of the dried gel precursors exhibited a wide endothermic peak in the range 323 K to 428 K (50 °C to 155 °C), which was attributed to the loss of moisture. A weak exothermic peak was observed at 476 K (203 °C), and immediately after that, a sharp exothermic peak was observed at approximately 560 K (287 °C), which indicates the completion of combustion of the fuel (citric acid)-nitrate precursor and crystallization of CeO₂. Almost no remarkable weight change was detected above 673 K (400 °C) in the TG curve, which indicates the formation of crystalline material. The same trends were also observed for ESDC, GSDC, and NSDC samples. The total weight loss is 66.2 pct.

B. XRD Analysis

Figure 2(a, b) shows the XRD patterns of the calcined and sintered SDC, ESDC, GSDC, and NSDC

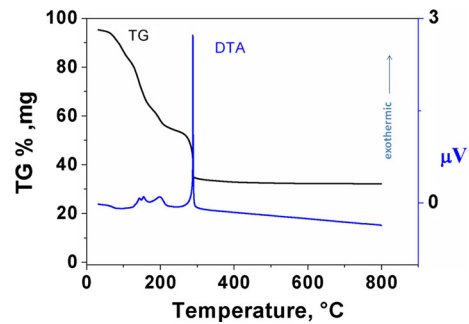


Fig. 1—TG–DTA curves of the thermal decomposition of Ce_{0.80}Sm_{0.20}O_{1.90} precursors at a heating rate of 5 K min⁻¹ (5°C min⁻¹) in air.

electrolyte samples. The XRD patterns show that all samples crystallize to a single phase with a cubic fluorite structure without any traces of Sm₂O₃, Er₂O₃, Gd₂O₃, or Nd₂O₃. The dissolution of the Sm₂O₃, Er₂O₃, Gd₂O₃, and Nd₂O₃ in the cubic fluorite lattice can cause small shifts in the ceria peaks because of the difference in ionic radii of Ce⁴⁺ (0.967 Å), Sm³⁺ (1.079 Å), Er³⁺ (1.004 Å), Nd³⁺ (1.109 Å), and Gd³⁺ (1.053 Å) in the lattice of CeO₂.

This shift implies a change in the lattice parameters. This situation confirms that all of the Nd³⁺, Gd³⁺, and Er³⁺ co-doped Sm-doped ceria electrolytes in this study form complete ceria-based solid solutions. The lattice parameter was in the range of 5.425–5.430 (Å). The crystallite sizes were calculated using Scherrer's Formula and found to be between 12.2 and 19.3 nm.

As shown in Figure 2(b), after sintering at 1673 K (1400 °C) all XRD peaks became sharper, indicating improved crystallinity and lattice stability.

C. FTIR Analysis

Figure 3 displays the FTIR transmission spectra of the calcined SDC, ESDC, GSDC, and NSDC powders and the sintered GSDC powders.

The spectra indicate some strong intense bands at approximately 3430 and 500 cm⁻¹. In addition, some weaker absorption peaks were also observed at approximately 2920, 1610, 1380, and 1050 cm⁻¹. In the range of 3000–3600 cm⁻¹, a band was attributed to the ν(O–H) vibration modes of the physically adsorbed water molecules. The weak peaks observed at approximately 2920 and 1610 cm⁻¹ were assigned to the ν(C–H) and δ(CH₂) vibration modes, respectively. These peaks originated from the presence of atmospheric organic components in the exposed samples during the sample preparation process. The peak observed at 1050 cm⁻¹ is generally attributed to the cerium–oxygen groups, which have a greater double bond character. The broad bands observed in the lower frequency region at 700 and 400 cm⁻¹ are typical of Ce–O groups having a lower double bond character and of Ce–O–Ce chains or Ce–O–R–E³⁺(R–E³⁺: Er³⁺, Nd³⁺, Gd³⁺, Sm³⁺) symmetric stretching of the metal oxide network.^[33,34]

The FTIR spectrum of the GSDC sample that was sintered at 1673 K (1400 °C) for 6 hours is shown in

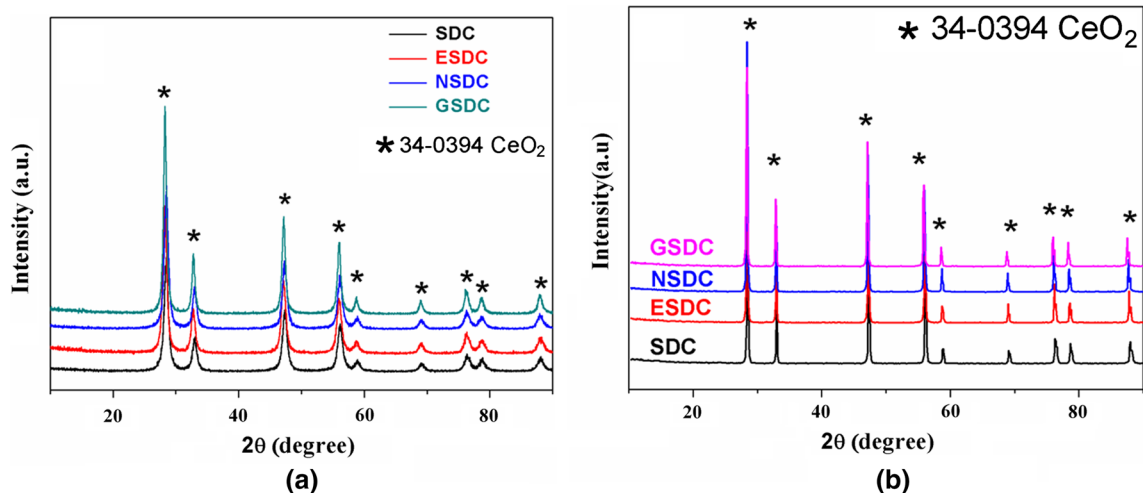


Fig. 2—XRD patterns of the calcined powders (a) and the sintered pellets (b) of SDC, ESDC, GSDC, and NSDC.

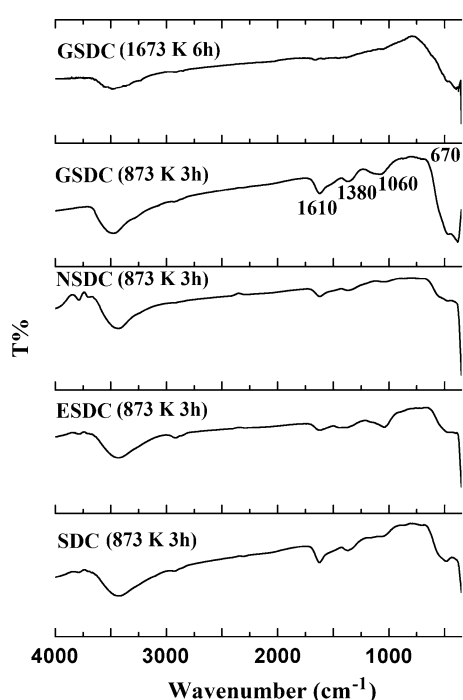


Fig. 3—FT-IR spectra of the calcined powders of SDC, ESDC, GSDC, and NSDC as well as GSDC powder sintered at 1673 K (1400 °C).

Figure 3. After sintering at 1673 K (1400 °C), the O–H stretching band was still observed at 3000 to 3600 cm^{-1} because of the water adsorbed during the KBr pellet preparation process; however, it had a lower intensity. The KBr salt can easily adsorb water molecules from the air *via* hydrogen bond formation on its surface. The FTIR spectra of the sintered sample indicated that the peaks at 2920, 1610, and 1380 cm^{-1} disappeared. The reason for this situation is thought to be the removal of residual carbonaceous materials. The broad band that corresponds to the cerium–oxygen bond is seen below 700 cm^{-1} . This result provides clear evidence for the formation of the RE (Er, Gd, Nd) and Sm co-doped

ceria.^[35] All sintered samples showed the same trend in the FTIR results. These results are consistent with the results from the DTA and X-ray diffraction analysis.

Figure 4 shows the scanning electron microscopy images of SDC, ESDC, GSDC, and NSDC pellets. After sintering at 1673 K (1400 °C) for 6 hours, all the sintered samples were composed of nearly fully dense structures and had uniform structure. It is clear that the surfaces and fracture surfaces of the samples are highly dense. This is in good agreement with the relative density (RD) of the samples. Because of the residual carbonaceous materials removed from the structure during calcination, a denser material was obtained after sintering. The densities of all the sintered pellets had nearly the same RD values, which were above 95 pct. However, the conventional solid-state method requires temperatures higher than 1773 K to 1873 K (1500 °C to 1600 °C) to obtain highly dense ceramics of Sm-doped ceria.^[36] The mean particle size of SDC was found to be 0.67 μm according to the SEM results. The mean particle sizes changed to 0.74, 0.78, and 0.81 μm when Gd, Nd, and Er, respectively, were added to SDC. The effects of Er, Nd, and Gd co-doping on the grain size of Sm-doped ceria electrolyte were observed to be slight. The gas evolution in a citric–nitrate combustion (CNC) process helps to limit the inter-particle contact and thus results in ultrafine powders with high purity and high sinterability. All samples prepared from the powders synthesized by the CNC process had good sinterability at 1673 K (1400 °C) and relatively uniform grain size distribution.

D. Ionic Conductivity

Impedance spectroscopy is a powerful tool to study the electrical properties of solid electrolytes and to analyze the grain, grain boundary, and electrode contributions to the overall ionic conductivity. In this work, the overall ionic conductivity of Nd^{+3} , Er^{+3} , and Gd^{+3} co-doped Sm-doped ceria materials is reported. In general, the total conductivity (σ_T) of ceria doped with

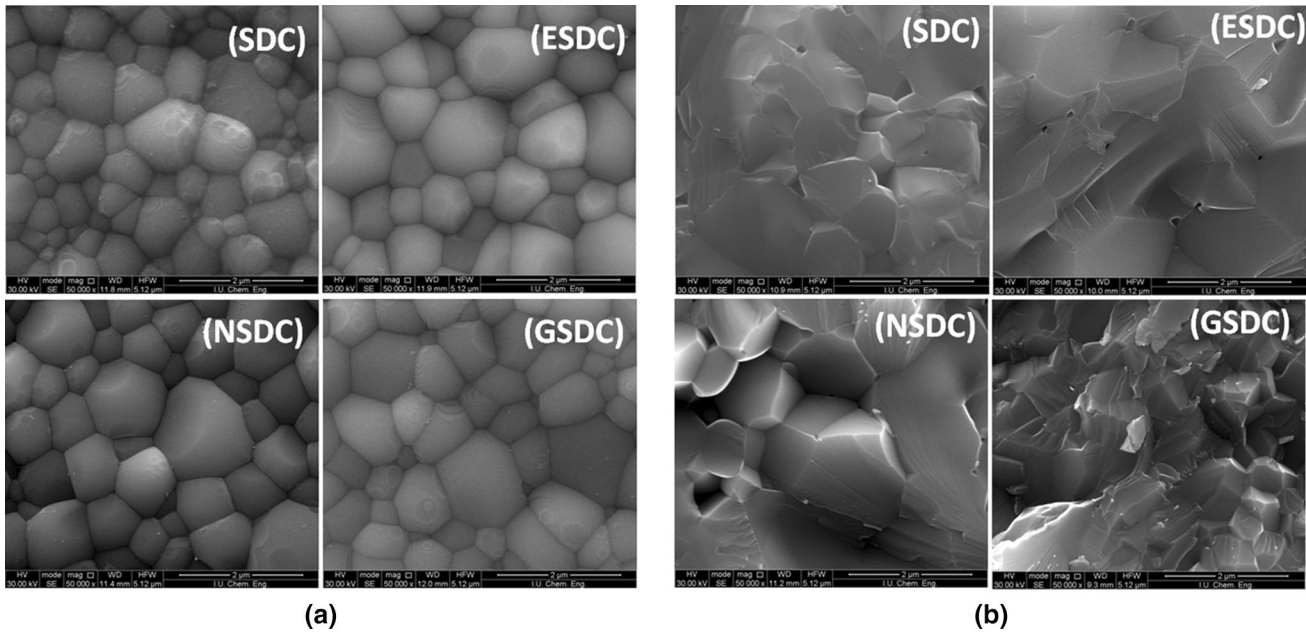


Fig. 4—SEM images of the surface (a) and cross-sectional fracture surfaces (b) of SDC, ESDC, GSDC, and NSDC pellets sintered at 1673 K (1400 °C) for 6 h.

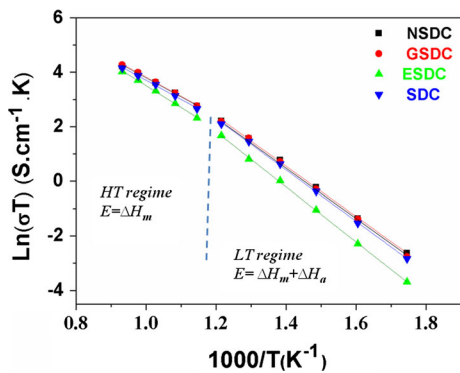


Fig. 5—Arrhenius plots for total ionic conductivity of SDC, ESDC, GSDC, and NSDC.

a rare earth element is the sum of the ionic conductivity (σ_i) and the electronic conductivity (σ_e). However, the main contribution of the conductivity of rare earth element-doped ceria in air is the ionic conductivity (σ_i), and the contribution of electronic conductivity (σ_e) is negligible [$\sigma_e \approx 10^{-5}$ S/cm < 1073 K (800 °C)].^[1,6,37,38] In this study, all measurements were performed at temperatures ≤ 1073 K (800 °C) in air.

Figure 5 shows the plots of $\ln(\sigma T)$ vs $1/T$ for the SDC, ESDC, GSDC, and NSDC samples sintered at 1673 K (1400 °C) for 6 hours. A change of slope at 773 K (500 °C) is observed in the Arrhenius plots, which indicates the presence of two activation energies ($\Delta H_m + \Delta H_a$, ΔH_m). This change depends on the change in the conduction mechanism at a specific temperature. In the low-temperature (LT) range 573 K to 773 K (300 °C to 500 °C), the activation energy (E_a) is the combination of the migration enthalpy (ΔH_m) and the defect association enthalpy (ΔH_a). However, in the

high-temperature (HT) range 773 K to 1073 K (500 °C to 800 °C), the activation energy is equal to only the migration energy (ΔH_m) because a large fraction of the oxygen vacancies are free to migrate.^[6,39] Similar results were previously reported by Zha *et al.*^[27] and Omar *et al.*^[40]

Figure 5 shows that the GSDC, NSDC, and SDC samples showed higher conductivities than the ESDC sample. The highest ionic conductivity value was found to be 5.28×10^{-2} S cm⁻¹ at 1023 K (750 °C) for GSDC. The activation energies for oxygen ion migration in the SDC, ESDC, GSDC, and NSDC electrolytes at different temperatures were calculated from the slope of $\ln(\sigma T) - 1/T$ plots. The conductivity data and activation energies are also presented in Table I. Among all samples, GSDC shows the highest ionic conductivity of 3.92×10^{-2} S cm⁻¹ at 973 K (700 °C), whereas ESDC shows the lowest ionic conductivity of 2.64×10^{-2} S cm⁻¹ at the same temperature. Ionic conductivity of the GSDC electrolyte is higher than those of the Ce_{0.8}Sm_{0.1}Mg_{0.1}O_{2- δ} (2.97×10^{-2} S cm⁻¹)^[41] and Ce_{0.8}Sm_{0.1}Y_{0.1}O_{1.9} (3.17×10^{-2} S cm⁻¹)^[42] electrolytes at 973 K (700 °C). The activation energy is minimal when there is no elastic strain present in the host lattice.^[8] To increase the ionic conductivity, the activation energy should be a minimum for oxygen diffusion.

The co-doping effect is drawing increasing attention in the field of SOFC electrolytes because of its advantage of higher electrical conductivity and lower activation energy. However, the mechanism of conductivity enhancement with co-doping process is not well understood. Some researchers^[1,8,9] demonstrated that the ionic conductivity of doped ceria is related to the lattice distortion. However, this theory cannot clarify the observation in the current study that Ce_{0.8}Gd_{0.08}Sm_{0.12}O_{1.90} has higher conductivity

Table I. Total Conductivities of Co-doped Ceria at Different Temperatures and Activation Energies

Sample	Conductivity (S cm ⁻¹)			Activation energy (eV)	
	973K (700 °C)	1023K (750 °C)	1073K (800 °C)	LT regime	HT regime
				573–773K (300–500 °C)	773–1073K (500–800 °C)
SDC	3.55×10^{-2}	4.71×10^{-2}	5.91×10^{-2}	0.81	0.70
ESDC	2.64×10^{-2}	3.90×10^{-2}	5.20×10^{-2}	0.80	0.86
NSDC	3.90×10^{-2}	5.26×10^{-2}	6.59×10^{-2}	0.79	0.63
GSDC	3.92×10^{-2}	5.28×10^{-2}	6.68×10^{-2}	0.80	0.60

than Ce_{0.8}Sm_{0.20}O_{1.90}, while the lattice constant of Ce_{0.8}Sm_{0.20}O_{1.90} (5.425 Å) is closer to that of pure ceria (5.411 Å) in comparison with that of Ce_{0.8}Gd_{0.08}Sm_{0.12}O_{1.90} (5.430 Å). Yamamura *et al.*^[10] observed that, in the Ce_{1-x-y}La_xM_yO_{2-δ} (M = Ca, Sr) system, the co-doping effect can suppress the ordering of oxygen vacancies, and thus can lower the activation energy and enhance the electrical conductivity. This hypothesis was also supported by Andersson *et al.*^[13] via theoretical calculation of the activation energy in the Sm³⁺ and Nd³⁺ co-doped ceria system. According to the experimental results in the current work, it can be inferred that by adding Sm³⁺ and Gd³⁺ together into ceria, more transferable oxygen vacancies can be created; moreover, the movement of oxygen vacancies in this co-doping structure becomes easier, and thus the ionic conductivity is enhanced.

The ionic conductivity results appear to be in good agreement with the Andersson's simulation work,^[13] where two selected combinations of Nd/Sm and Gd /Sm both show enhanced ionic conductivity compared with those of Ce_{0.8}Sm_{0.2}O_{1.9} and Ce_{0.8}Er_{0.08}Sm_{0.12}O_{1.90} (see Figure 5). The average atomic numbers are 61 and 63 for Nd/Sm and Gd /Sm, respectively. These values are close to the atomic numbers of Pm (61) and Sm (62), which can be defined as the ideal dopants that exhibit low activation energy for oxygen diffusion and high ionic conductivity, as proposed by Andersson *et al.*^[13] Thus, it was assumed that the potential oxygen vacancies that facilitate the migration of oxygen ions in the ceria lattice increased. This situation increased the ionic conductivity of the electrolyte material.

IV. CONCLUSIONS

Neodymium, erbium, and gadolinium co-doped Sm-doped ceria samples were successfully synthesized using the CNC method. Dense ceramics were obtained by sintering the pellets at 1673 K (1400 °C) for 6 hours. The relative densities were over 95 pct of the theoretical density, and these results are consistent with the SEM studies. The combustion process is suitable for synthesizing complex oxide powders of high compositional homogeneity and high purity, which is advantageous over the conventional solid state method. The XRD patterns of the samples prepared with the CNC method exhibited the fluorite structure of CeO₂.

In accordance with the results of ionic conductivity, two of the co-dopants, Nd and Gd, increased the electrical conductivity of the SDC electrolyte, and the

maximum value was observed for Gd co-doped SDC. The ionic conductivity results showed that Er addition into SDC reduced the ionic conductivity of SDC. The ionic conductivity value of GSDC was found as 5.28×10^{-2} S cm⁻¹ at 1023 K (750 °C), which is 12 pct higher than that of Gd-free SDC. Because of this higher ionic conductivity, GSDC is a better material for IT-SOFC applications than SDC.

ACKNOWLEDGMENTS

This work was financially supported by the Research Fund of Istanbul University.

REFERENCES

1. B.C.H. Steele: *Solid State Ion.*, 2000, vol. 129 (1–4), pp. 95–110.
2. V.V. Kharton, F.M.B. Marques, and A. Atkinson: *Solid State Ion.*, 2004, vol. 174 (1–4), pp. 135–49.
3. J.B. Goodenough: *Annu. Rev. Mater. Res.*, 2003, vol. 33, pp. 91–128.
4. L. Anna and S.J. Skinner: *J. Mater. Chem.*, 2006, vol. 16, pp. 3161–70.
5. X. Sha, Z. Lü, X. Huang, J. Miao, Z. Ding, X. Xin, and W. Su: *J. Alloys Compd.*, 2007, vol. 428 (1–2), pp. 59–64.
6. H. Inaba and H. Tagawa: *Solid State Ion.*, 1996, vol. 83 (1–2), pp. 1–16.
7. S. Kuharuangrong: *J. Power Sources*, 2007, vol. 171 (2), pp. 506–10.
8. H. Yahiro, Y. Eguchi, K. Eguchi, and H. Arai: *J. Appl. Electrochem.*, 1988, vol. 18 (4), pp. 527–31.
9. D.J. Kim: *J. Am. Ceram. Soc.*, 1989, vol. 72, pp. 1415–21.
10. H. Yamamura, E. Katoh, M. Ichikawa, K. Kakinuma, T. Mori, and H. Haneda: *Electrochemistry*, 2000, vol. 68, pp. 455–59.
11. S. Ramesh, V.P. Kumar, P. Kistaiah, and C.V. Reddy: *Solid State Ion.*, 2010, vol. 181 (1–2), pp. 86–91.
12. F.Y. Wang, B.Z. Wan, and S. Cheng: *J. Solid State Electrochem.*, 2005, vol. 9 (3), pp. 168–73.
13. D.A. Andersson, S.I. Simak, N.V. Skorodumova, I.A. Abrikosov, and B. Johansson: *PNAS*, 2006, vol. 103 (10), pp. 3518–21.
14. T. Mori, J. Drennan, J.H. Lee, J.G. Li, and T. Ikegami: *Solid State Ion.*, 2002, vol. 154 (155), pp. 461–66.
15. J. Van Herle, D. Seneviratne, and A.J. McEvoy: *J. Eur. Ceram. Soc.*, 1999, vol. 19, pp. 837–41.
16. F.Y. Wang, S. Chen, Q. Wang, S. Yu, and S. Cheng: *Catal. Today*, 2004, vol. 97 (2–3), pp. 189–94.
17. H. Yoshida, T. Inagaki, K. Miura, M. Inaba, and Z. Ogumi: *Solid State Ion.*, 2003, vol. 160, pp. 109–16.
18. H. Yoshida, H. Deguchi, K. Miura, and M. Horiuchi: *Solid State Ion.*, 2001, vol. 140, pp. 191–99.
19. R.K. Lenka, T. Mahata, A.K. Tyagi, and P.K. Sinha: *Solid State Ion.*, 2010, vol. 181 (5–7), pp. 262–67.
20. T. Mori and J. Drennan: *J. Electroceram.*, 2006, vol. 17 (2–4), pp. 749–57.

21. K.C. Anjaneya, G.P. Nayaka, J. Manjanna, G. Govindaraj, and K.N. Ganesha: *J. Alloys Compd.*, 2013, vol. 578, pp. 53–59.
22. T.S. Zhang, J. Ma, L.B. Kong, S.H. Chan, and J.A. Kilner: *Solid State Ion.*, 2004, vol. 170 (3–4), pp. 209–17.
23. M. Mogensen, N.M. Sammes, and G.A. Tompsett: *Solid State Ion.*, 2000, vol. 129, pp. 63–94.
24. B. Li, Y. Liu, X. Wei, and W. Pan: *J. Power Sources*, 2010, vol. 195, pp. 969–76.
25. H.C. Yao, Y.X. Zhang, J.J. Liu, Y.L. Li, J.S. Wang, and Z.J. Li: *Mater. Res. Bull.*, 2011, vol. 46, pp. 75–80.
26. A. Arabaci, V. Sariboğa, and M.A.F. Öksüzömer: *Metall. Mater. Trans. A*, 2014, vol. 45A, pp. 5259–69.
27. S. Zha, C. Xia, and G. Meng: *J. Power Sources*, 2003, vol. 115 (1), pp. 44–48.
28. B. Xia, I.W. Lenggoro, and K. Okuyama: *J. Mater. Chem.*, 2001, vol. 11 (12), pp. 2925–27.
29. R.D. Purohit, B.P. Sharma, and K.T. Pillai: *Mater. Res. Bull.*, 2001, vol. 36 (15), pp. 2711–21.
30. T. Mahata, G. Das, R.K. Mishra, and B.P. Sharma: *J. Alloys Compd.*, 2005, vol. 391 (1–2), pp. 129–35.
31. R.K. Lenka, T. Mahata, P.K. Sinha, and B.P. Sharma: *J. Am. Ceram. Soc.*, 2006, vol. 89 (12), pp. 3871–73.
32. K. Channa, R. De Silva, Brian.J. Kaseman, and D.J. Bayless: *Int. J. Hydrogen Energy*, 2011, vol. 36 (6), pp. 779–86.
33. C. Ho, J.C. Yu, T.A. Kwong, C. Mak, and S. Lai: *Chem. Mater.*, 2005, vol. 17, pp. 4514–22.
34. J.J. Ketzial and A.S. Nesaraj: *J. Ceram. Process. Res.*, 2011, vol. 12, pp. 74–79.
35. S. Kundu, N. Sutradhar, R. Thangamuthu, B. Subramanian, A.B. Panda, and M. Jayachandran: *J. Nanopart. Res.*, 2012, vol. 14, pp. 1040–56.
36. S. Omer, E.D. Wachsman, and J.C. Nino: *Solid State Ion.*, 2006, vol. 177, pp. 3199–3208.
37. J.A. Kilner: *Solid State Ion.*, 2000, vol. 129, pp. 13–23.
38. W. Lai and S.M. Haile: *J. Am. Ceram. Soc.*, 2005, vol. 88 (11), pp. 2979–97.
39. H. Li, C. Xia, M. Zhu, Z. Zhou, and G. Meng: *Acta Mater.*, 2006, vol. 54, pp. 721–27.
40. S. Omar, E.D. Wachsman, and J.C. Nino: *Solid State Ion.*, 2008, vol. 178, pp. 1890–97.
41. Y. Zheng, H. Gu, H. Chen, L. Gao, X. Zhu, and L. Guo: *Mater. Res. Bull.*, 2009, vol. 44, pp. 775–79.
42. X. Sha, Z. Lü, X. Huang, J. Miao, L. Jia, and X. Xin: *J. Alloys Compd.*, 2006, vol. 424, pp. 315–21.